COBEM 2023 27TH INTERNATIONAL CONGRESS OF MECHANICAL ENGENEERING

ABCM Brazilian Society of Mechanical Sciences and Engineering
27th ABCM International Congress of Mechanical Engineering
December 04-08, 2023, Florianópolis-SC, Brazil

COB-2023-0394 MODELING AN ELECTROSPRAY PROPULSION SYSTEM USING AN OPEN-SOURCE SMOOTHED PARTICLE HYDRODYNAMICS METHOD

Marcelo dos Santos Ferreira
Marco Antonio Gontijo Piantino
Ricardo Adriano
Universidade Federal de Minas Gerais (UFMG) - Av. Antônio Carlos, 6627, Pampulha - Belo Horizonte - MG - CEP 31270-901
marcelosferreira@ufmg.br
piantinom@ufmg.br
rluiz@ufmg.br

Diogo Leon Oliveira Soares
Laboratório de Propulsão Elétrica Espacial - Laboratório Associado de Combustão e Propulsão, Coordenação de Pesquisa Aplicada e Desenvolvimento Tecnológico - Coordenação-Geral de Infraestrutura e Pesquisas Aplicadas, Instituto Nacional de Pesquisas Espaciais - Rodovia Presidente Dutra km 40, Cachoeira Paulista - SP
diogo.leon@inpe.br

Alexandre Ramos Fonseca
Universidade Federal dos Vales do Jequitinhonha e Mucuri (UFVJM) - Rodovia MGT 367 – Km 583, nº 5000, Alto da Jacuba, Diamantina/MG
arfonseca@ufvjm.edu.br

Abstract. *Electrospray Thrusters are being investigated by many researchers because of their small size, which is suitable for small spacecraft. Different models have been proposed in the literature, including simple analytical models with limited accuracy and more complex weak-coupled Electromagnetic Fluid Dynamic numerical approaches. However, accurate and time efficient solutions are still unavailable. To address this problem, this paper proposes an open-source Python tool based on the Smoothed Particle Hydrodynamics (SPH) method. SPH is a Lagrangian mesh-free approach that can naturally incorporate fluid dynamics physical effects, and it has been successfully applied to many fluid dynamics problems, such as free surface flow and electrophoretic deposition. The proposed tool aims to balance efficiency, simplicity, and code reuse. The Navier-Stokes governing equations can be represented in state-space form, and they can be efficiently solved using the open-source Scientific Computing Python Library. This library provides a variety of Initial Value Problem solvers, making it well-suited for performing the SPH integration scheme. The tool is validated using the Poiseuille Flow Problem, where analytical solutions are available to check the accuracy and performance of the different SciPy solvers. Computational aspects, including the neighbor particle search and surface detection, are also investigated. The results obtained using different particle numbers showed good agreement with the analytical velocity profile, with errors ranging from 3% to 12%, depending on the particle number. Finally, the tool is validated and a simplified bidimensional planar Electrospray Thrusters model is simulated.*

Keywords: *Electric Thruster, Navier-Stokes Equations, Multiphysics Simulation, Meshfree Methods.*

1. INTRODUCTION

In recent decades Electric Propulsion (EP) has becoming popular worldwide for spacecrafts missions on defense, commercial and space science (Lev *et al.*, 2019). Many different electromagnetic acceleration mechanisms have been created, some of them generating moderate to high thrust level (Mazouffre, 2016) (compared to others EP devices) and others with low thrust levels as electrospray thrusters (ET) (O'Reilly *et al.*, 2021). The ET are micropropulsion systems used for accurate maneuvers in nanosat, cubesat (Mazouffre, 2016) and are of interest for many researchers nowadays (Wirz, 2019; Chong *et al.*, 2020; Uchizono *et al.*, 2021; Thuppul *et al.*, 2020). They can be defined as electrostatic accelerators of charged droplets or of ions extracted directly from a liquid (Lozano *et al.*, 2010). A schematic diagram of a simple electrospray is shown in Figure 1.

The physics of the ET can be briefly described as follows: When an electric field is applied to a conductive liquid (propellant), charged particles are attracted to its surface, from a threshold electric field value the surface becomes unstable (Lozano *et al.*, 2010). The radial electric field creates the shear stress on the liquid surface by the tangential pulling force on the ions and the liquid is accelerated to the apex of the electrospray (Lozano *et al.*, 2010) forming the Taylor

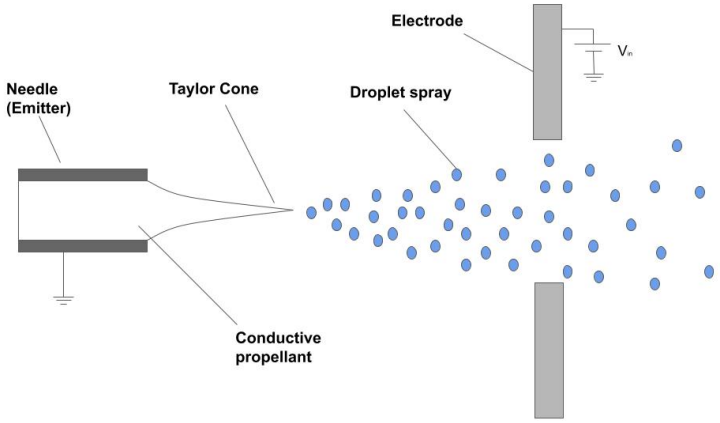

Figure 1. Schematic diagram of an electrospray thruster.

cone. The liquid at the apex is ejected in the form of a thin jet, a stream of ions or a mixture of both (Lozano *et al.*, 2010) which can form the droplets as it is depicted in Figure 1.

For a deeper understanding on the physics of the ET, researchers have been working on different models. These models range since analytical methods (Xue *et al.*, 2021; Gamero-Castaño, 2008) to more complex numerical approaches including volume of fluid method (Huh and Wirz, 2019), finite difference method (Legge Jr, 2008) and molecular dynamics (MD) simulation (Kim and Micci, 2013; Asher *et al.*, 2022). Although the MD models are accurate describing the performance and the physical behavior of the thruster, the computational effort is highly demanded due to the number of particles needed. Concerning this issue, the meshfree particle method *Smoothed Particle Hydrodynamics* (SPH) (Liu and Liu, 2003) is suggested by the authors of this work as an alternative, as this meshfree method simulates particles in the domain at the same time holding the continuum feature of the Navier-Stokes Equations that may lead to a number of particles smaller than the MD simulation requires. Furthermore, as a particle method, SPH has the advantage, compared to the usual grid methods, in dealing with free surface, moving surface, deformable boundary and large deformation (Liu and Liu, 2010).

In order to validate the SPH algorithm the Poiseuille Flow Problem was used, where the incompressible flow is induced by pressure gradient inside a duct, forming a parabolic velocity profile in steady-state condition (White, 1966). The analytical solution is used to assess the accuracy and the performance of the solvers. The deviation from the analytical solution associated with the Poiseuille Flow for the steady-state velocity profile surrounded 3% to 12% depending on the particle number. Finally, the tool is validated and a simplified bidimensional planar Electrospray Thrusters model is simulated.

1.1 Physical background

The electrospray physics is governed by a Newtonian viscous isothermal fluid flow induced by an electrical field generated due an electrical potential difference between the emitter and the electrode, as represented by the Figure 1. The governing equations of the fluid mechanics of Newtonian viscous isothermal flow in the Lagrangian frame of reference are described as below (Kundu *et al.*, 2015; Hu *et al.*, 2021):

$$\frac{D\rho}{Dt} = -\rho\nabla\cdot\mathbf{v}, \tag{1}$$

$$\frac{D\mathbf{v}}{Dt} = -\frac{1}{\rho}\nabla p + \frac{1}{\rho}\left\{\nabla\cdot(\mu\nabla\mathbf{v})\right\} + \mathbf{F}^{(\mathbf{s})} + \mathbf{F}^{(\mathbf{b})}, \tag{2}$$

where ρ is the density of the fluid, $\mathbf{v}$ is velocity vector, p is the mean pressure, μ is the dynamic viscosity, $\mathbf{F}^{(\mathbf{s})}$ are the surface forces, $\mathbf{F}^{(\mathbf{b})}$ are the body forces and the operator $\frac{D}{Dt} = \frac{\partial}{\partial t} + \mathbf{v}\cdot\nabla$ is the material derivative (Kundu *et al.*, 2015; Hu *et al.*, 2021).

The surface forces $\mathbf{F}^{(\mathbf{s})}$ play an important role in this work due to the surface tension. The surface tension is one of the main phenomena responsible for the Taylor cone formation and must receive special attention in the modeling as other authors detailed (Adami *et al.*, 2010; Breinlinger *et al.*, 2013; Sun *et al.*, 2021). Physically the surface tension is modeled by the continuum surface force (Brackbill *et al.*, 1992) as described by Eq.(3) (Brackbill *et al.*, 1992; Sun *et al.*, 2021):

$$\mathbf{F}^{(\mathbf{s})} = -\gamma\kappa\mathbf{n}\delta_{\mathbf{\Sigma}}, \tag{3}$$

where γ is the surface tension coefficient and it is a physical property of the fluid, κ is the curvature, $\mathbf{n}$ is the normal vector of the free surface and δ_{Σ} is a delta function that limits the regions of the body forces to the vicinity of the boundaries (Sun *et al.*, 2021).

The only body force $\mathbf{F^{(b)}}$ considered in the simulation of this work is the electrostatic force $\mathbf{F^{(e)}}$. As the time scale of the problem is small, the gravitational acceleration does not play an import role in the *momentum* balance (Eq. (2)), hence it is not considered.

The electrodynamic problem of the electrospray is dominated by the electrostatic field generated by the electric potential difference between the electrodes and the emitter, as the current involved in the propellant emission is very low, in the order of μA (Chong *et al.*, 2020) resulting in low induced magnetic effects (Hu *et al.*, 2021), and the electric potential difference between the emitter and the electrodes is high, in the order of kV (Chong *et al.*, 2020). The set of equations that governs the phenomenon are the Faraday's Law, Gauss Law and the charge conservation equation as stated in the following equations (Machado, 2007; Reitz, 2009):

$$\nabla \times \mathbf{E} = 0, \tag{4}$$

$$\nabla \cdot \mathbf{E} = \frac{\rho_e}{\epsilon}, \tag{5}$$

$$\frac{\partial \rho_e}{\partial t} + \nabla \cdot \mathbf{J} = 0, \tag{6}$$

where ρ_e is the charge distribution, $\mathbf{E}$ is the electrostatic field, ϵ is the electric permittivity of the medium and $\mathbf{J}$ is the current density (Machado, 2007). The current density is the sum of the ohmic charge conduction and the charge convection (Huh and Wirz, 2019)

$$\mathbf{J} = \sigma \mathbf{E} + \rho_e \mathbf{v}, \tag{7}$$

where σ is the conductivity of medium. Equations (4) to (7) are coupled to Eq. (1) and Eq. (2) by the velocity and the Electrostatic force $\mathbf{F}_e$ represented by the summation of Coulombic and polarization force

$$\mathbf{F}_e = \rho_e \mathbf{E} - \frac{1}{2} E^2 \nabla \epsilon. \tag{8}$$

In this work, a simplified version considering low conductivity fluids applies. In this case polarization force is dominant, allowing the electrodynamic problem to be reduced to the electrostatic Laplace equation:

$$\nabla \cdot \epsilon \nabla \phi = 0, \tag{9}$$

where ϕ represents the electric potential, while the excitation of the homogeneous equation arises from the voltage applied between the electrode and the emitter, acting as a Dirichlet condition.

In this case, the fluid dynamic problem is connected to the electrostatic problem only through the polarization force. Thus, the problems can be solved separately. Firstly, the electrostatic problem is solved, and $\mathbf{F}_e$ is determined. In a second step, the fluid dynamic problem is solved, with the previously found force serving as the excitation one. To solve the electrostatic problem, the FEniCS platform is used (Logg *et al.*, 2012). FEniCS allows to solve Eq. (9) using a high-level Python language, making it easier to communicate with the proposed SPH solution.

2. THE SPH IMPLEMENTATION

The SPH equation are obtained to the fluid mechanics governing equations, Eq. (1) and Eq. (2) resulting in (Liu and Liu, 2003):

$$\frac{D\rho_i}{Dt} = \sum_{j=1}^{N} m_j \mathbf{v}_{\mathbf{ij}}^{\beta} \cdot \frac{\partial \mathbf{W_{ij}}}{\partial \mathbf{x}_{\mathbf{i}}^{\beta}}, \tag{10}$$

$$\frac{Dv_i^{\alpha}}{Dt} = -\sum_{j=1}^{N} m_j \left(\frac{p_i}{\rho_i^2} + \frac{p_j}{\rho_j^2} \right) \frac{\partial W_{ij}}{\partial x_i^{\alpha}} + \sum_{j=1}^{N} m_j \left(\frac{\mu_i \varepsilon_i^{\alpha\beta}}{\rho_i^2} + \frac{\mu_j \varepsilon_j^{\alpha\beta}}{\rho_j^2} \right) \frac{\partial W_{ij}}{\partial x_i^{\beta}} + F^{\alpha}(t), \tag{11}$$

where

$$\varepsilon_i^{\alpha\beta} = \sum_{j=1}^{N} \frac{m_j}{\rho_j} v_{ji}^{\beta} \frac{\partial W_{ij}}{\partial x_i^{\alpha}} + \sum_{j=1}^{N} \frac{m_j}{\rho_j} v_{ji}^{\alpha} \frac{\partial W_{ij}}{\partial x_i^{\beta}} - \left(\frac{2}{3} \sum_{j=1}^{N} \frac{m_j}{\rho_j} v_{ji} \cdot \nabla_i W_{ij} \right) \delta^{\alpha\beta}. \tag{12}$$

The parameter $\varepsilon_i^{\alpha\beta}$ is the strain rate tensor (Liu and Liu, 2003), $v_{ij}^{\beta} = v_i^{\beta} - v_j^{\beta}$ is the relative velocity between the particles j and i, $\delta^{\alpha\beta}$ is the Kronecker delta (Kundu *et al.*, 2015), and $F^{\alpha}(t)$ is the sum of body $F^{\alpha(b)}(t)$ and surface forces $F^{\alpha(s)}(t)$ in the α direction.

For incompressible fluid problems it is usual the implementation of the artificial compressibility. It is based on the fact that every fluid is slightly compressible (Liu, 2009) and it is modeled by the following equation (Monaghan, 1994):

$$p = B \left[\left(\frac{\rho}{\rho_0} \right)^{\gamma} - 1 \right]. \tag{13}$$

2.1 Surface Tension

In order to apply the surface tension model described by Eq. (3), it is essential to identify properly the free surface of the fluid. Other authors have proposed free surface detection for the SPH method (Adami *et al.*, 2010; Lin *et al.*, 2019; Sun *et al.*, 2021) and in this work the arc-method is used (Sun *et al.*, 2021). In the arc-method a circle is created with its center located at the reference particle with the radius equals to the initial particle spacing. For each neighboring particle inside the support domain of the reference particle, circles are also created and checked whether it intersects the reference particle circle. When an arc of the reference particle circle does not lie inside the neighboring particle circle then it is considered a free surface particle. Otherwise it is considered an inner particle (Sun *et al.*, 2021). Figure 2 describes graphically the arc-method.

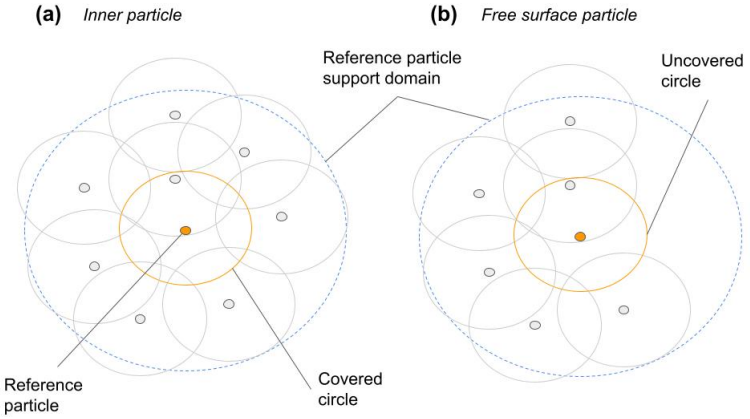

Figure 2. Criteria for free surface particle and inner particle search. In (a) inner particle and (b) free surface particle.

For each free surface particle, the curvature κ in Eq. (3) is evaluated as:

$$\kappa = \frac{1}{R_c}, \tag{14}$$

where R_c is the radius of the circumcircle of the reference particle and other two adjacent free surface particles (Sun *et al.*, 2021). The normal vector, also presented in Eq. (3), is computed normalizing the vector connecting the the circumcenter to the particle. Alternatively, it can be calculated using the mean between the vectors connecting the free particle to the adjacent ones, as described in Sun *et al.* (2021). Both methods present similar results and only the first one is adopted in this paper. Then, based on the methodology of Brackbill *et al.* (1992) and Sun *et al.* (2021), the following equation was implemented in the algorithm to represent the surface tension:

$$F^{\alpha(s)}(t) = -\frac{\gamma \kappa n^{\alpha}}{\Delta H}, \tag{15}$$

where n^{α} is the component in the α direction of the normal vector and ΔH is the initial particle spacing.

2.2 The SPH state-space representation

To simultaneously solve Eq. (10), Eq. (11) and the particle position update equation

$$\frac{Dx_i^{\alpha}}{Dt} = v_i^{\alpha}, \tag{16}$$

the governing equations are presented as state-space representation. Defining the vector of state variables as $y = (\rho_i, x_i^{\alpha}, v_i^{\alpha})$, the system of equations can be rewritten as:

$$\dot{\rho}_i = f(y), \tag{17}$$
$$\dot{x}_i^{\alpha} = v_i^{\alpha}(t), \tag{18}$$
$$\dot{u}_i^{\alpha} = g(y) + F(t), \tag{19}$$

or alternatively:

$$\dot{y} = f'(y, t), \tag{20}$$

where $f'(y, t)$ can be efficiently solved using the *solve-ivp* function from the open-source Scientific Computing Python Library (Scipy, 2023). Scipy offers a wide range of Initial Value Problem (IVP) solvers for performing the SPH integration scheme, leading to a compact and fast code.

2.3 The particle search scheme

Regarding the computational aspects, the search algorithm adopted in this work uses a two-dimensional hash table to store the neighborhood of particles. It has an order of $O(N_p)$ for particle sorting and a storage cost of $(N_g \times N_{pc})$, where N_p is the total number of particles, N_g is the number of grid cells, and N_{pc} is the average number of particles in each cell. Although more advanced techniques involving data compression already exist in the literature (Band *et al.*, 2020), the implemented method offers a good balance between efficiency and simplicity. The sorting algorithm is illustrated in Figure 3.

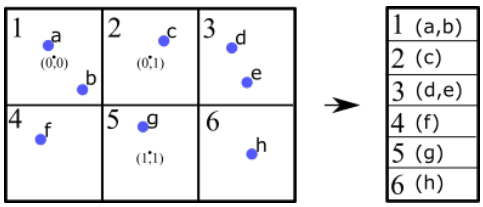

Figure 3. Example of building the two-dimensional hash table.

In Figure 3, the domain is divided into a (2x3) grid containing approximately 1.5 elements per cell. Thus, a (6x2) table is created where each row stores the elements of the cell. The table is constructed by looping through all the elements. The index of each element is obtained by rounding the position of each particle with a precision equal to the grid spacing.

Once the table is built, the search for neighboring particles is only performed in the adjacent cells that share some interface with the box containing the support domain of the particle, as shown in Figure 4. In this example, cells 2, 3, 5 and 6 are used to identify the neighboring particles of particle e. They can be easily identified by examining the cells that contain the vertices of the searching box.

Since the fluid moves into the space, the hash table must be updated from time to time. In this paper, the table is reconstructed for every time step. The size of the grid containing the particles is redefined at each time step based on the particles at the outermost edges plus the smoothing length h. The number of grid cells may impact the performance of the method. This is illustrated in the result section.

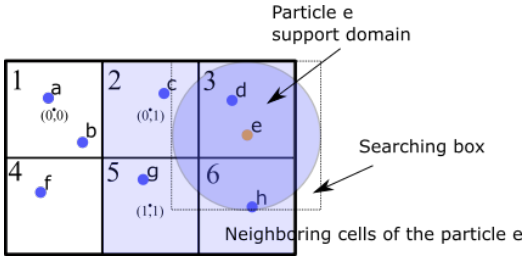

Figure 4. Neighboring cells of particle e.

3. RESULTS AND DISCUSSION

3.1 Poiseuille Flow

The Poiseuille Flow is a flow driven by pressure gradient between two fixed plates. The solution to this problem is analytical in steady-state condition and it can be written in form of a series function for the transient problem (Morris *et al.*, 1997):

$$u_x(z,t) = \frac{F}{2\nu} z(z-l) + \sum_{n=0}^{\infty} \frac{4Fl^2}{\nu\pi^3(2n+1)^3} sin\left[\frac{\pi z}{l}(2n+1)\right] exp\left[-\frac{(2n+1)^2\pi^2\nu}{l^2}t\right], \tag{21}$$

where ν is the kinematic viscosity, $l = 1$ mm is the height of the rectangular channel and $F = 0.0002$ m/s^2 is the driven force exerted on the particles.

In order to verify the performance of the Poiseuille Flow algorithm, it was evaluated different configuration parameters, including: different amount of particles in the y-axis, varying from 11 to 101 particles and different types of time integration methods available in the SciPy library. The integration methods used were: Explicit Runge-Kutta methods ($RK45$, $RK23$, $DOP853$), Implicit Runge-Kutta method ($Radau$), Implicit multi-step variable-order method (BDF) and Adams BDF method with automatic stiffness detection ($LSODA$).

As illustrated in Figure 5 and Figure 6, the implicit methods ($Radau$, BDF, $LSODA$) executed in less time and had better quality results than the explicit ones.

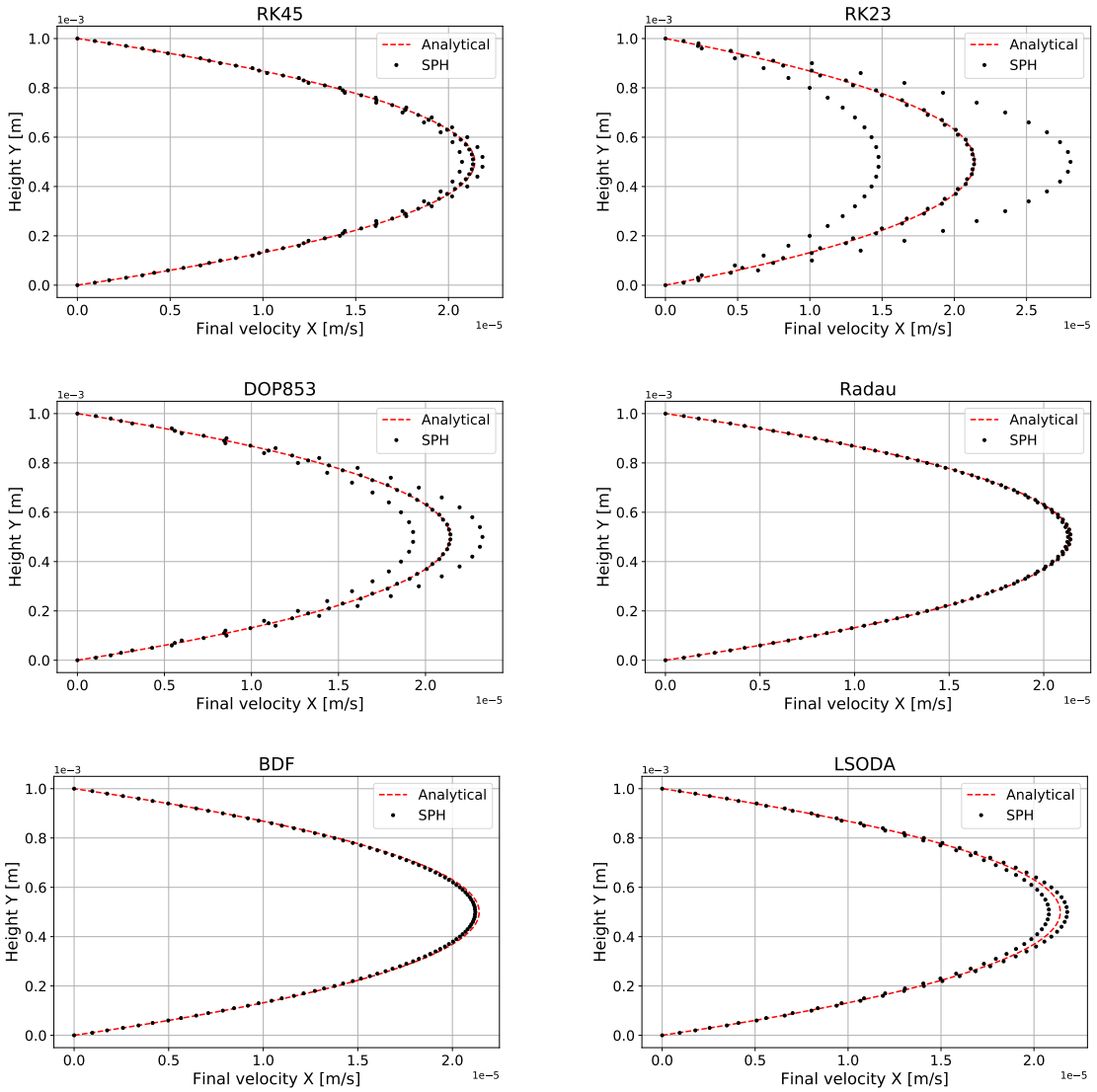

Figure 5. Comparison of velocity profile between analytical solution and SPH.

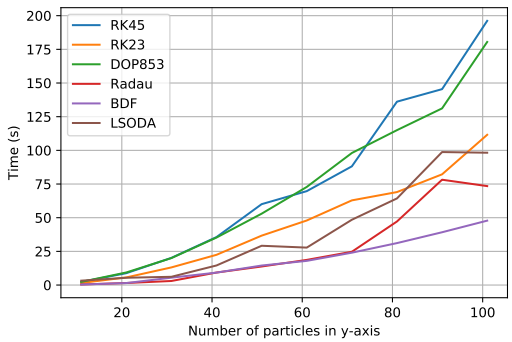

Figure 6. Simulation results of the Poiseuille Flow for 8 cells in the y-axis.

3.2 Initially squared droplet test

In order to verify the surface tension described in section 2.1, this test replicates the results of section 5.2 of Sun *et al.* (2021). The deformation process of an initially squared droplet is investigated. The fluid density is 1000 kg/m^3 and the dynamic viscosity is $0.1\text{Pa} \cdot \text{s}$. The side length of the droplet is 1 cm and the surface tension coefficient is 0.025N/m. This problem is more challenging than the previous one because it requires a true two-dimensional domain. Additionally,

the results are easy to interpret since the final position of the droplet is well-known.

A total of 41×41 particles are used in this test. Different from the Poiseuille Flow, the implicit methods had poor performance and impracticable time execution compared to the explicit ones. For this reason, implicit methods were not used in this problem. Table 1 shows the computational time for different explicit methods and number of grid cells. The results show little variation regarding the grid size.

Table 1. Simulation results for 41 x 41 particles.
Time in seconds

Number of grid cells in the x-axis y-axis	$RK45$	$RK23$	$DOP853$
4	7223	5897	8204
8	6972	5860	8147
16	6860	5791	7616

Figure 7 presents the initial and final solution ($t = 0.2s$) of the problem. It is possible to see that some inner particle are misidentified as free surface particle. This happened because the arc-method implemented in this paper only compare the intersections between two adjacent neighbours and may fail if a portion of the reference particle circle is covered by non-adjacent neighbours particles. That was done in order to prioritize performance over the accuracy of the detection method. Results presented in (Sun *et al.*, 2021) show that false detection of isolated points within the fluid does not affect the method's performance significantly.

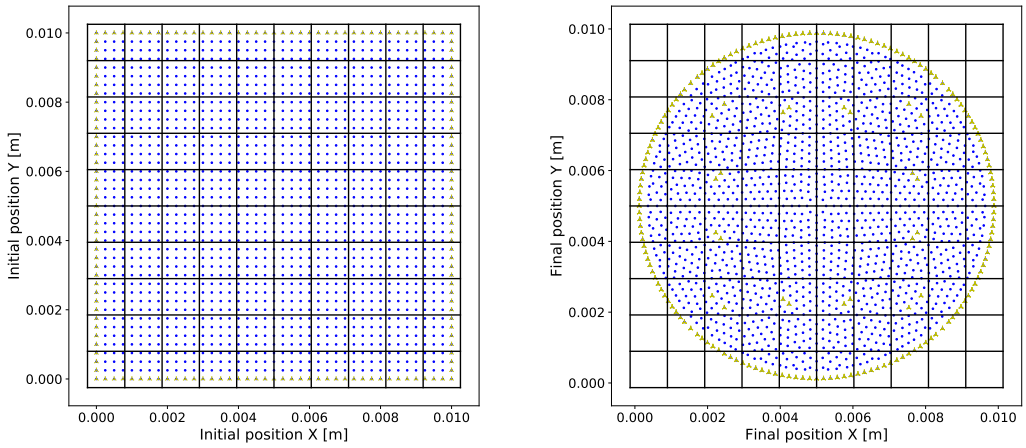

Figure 7. Initial and final position of the square droplet problem. Particles in blue are internal particles while yellow particles are detected as free surface.

3.3 Electrospray simulation

In the last problem, the electrospray thruster of Figure 1 is solved assuming planar symmetry. The emitter gap was adjusted to $D = 0.1\text{mm}$, while the gap between the electrode plates was set to 2.0mm. The electrode is positioned 1.3mm away from the emitter and the applied voltage was equal to 8kV.

The fluid under consideration is the Heptane, with properties such as relative permittivity equal to 2, density equal to 684kg/m^3, viscosity equal to $0.389\text{mPa} \cdot \text{s}$ and surface tension equal to 0.021N/m. First, the electrostatic problem is solved using FEniCs. The fluid tip is terminated on a circular surface with a diameter equal to the emitter opening (D), forming a droplet at the emitter outlet. This condition is used to determine the Electric field at the tip of the droplet E_n, considering the applied voltage. The result is presented in Fig 8. In this case, the resulting electric field (E_n) is equal to 9.25MV/m.

Once the field is obtained, the SPH problem is solved. The electric force is approximated on Eq. (11) as an uniformly distributed body force, mathematically:

$$F_E = \frac{\epsilon_0 E_n^2}{2D\rho_i}\hat{x}. \tag{22}$$

Figure 9 shows the results obtained using 21×21 particles. The state-space problem was solved using the RK45 method with default configurations. In the figure, particles in blue are internal particles while yellow particles are detected

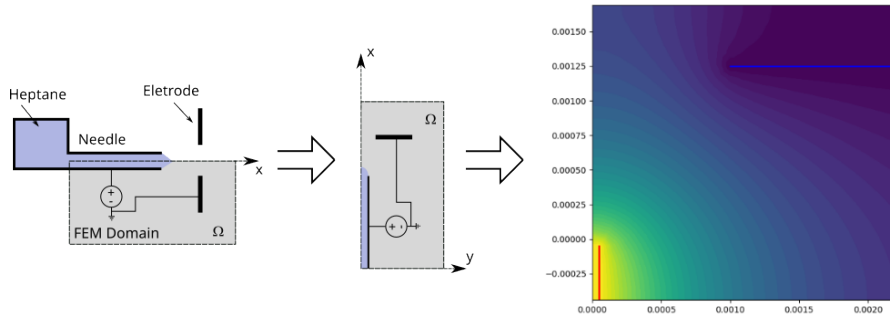

Figure 8. Electric potential obtained using FEniCS with 2482 first order triangular elements.

as free surface. The black particles represent the interface with the emitter where the acceleration was force to zero during the entire simulation.

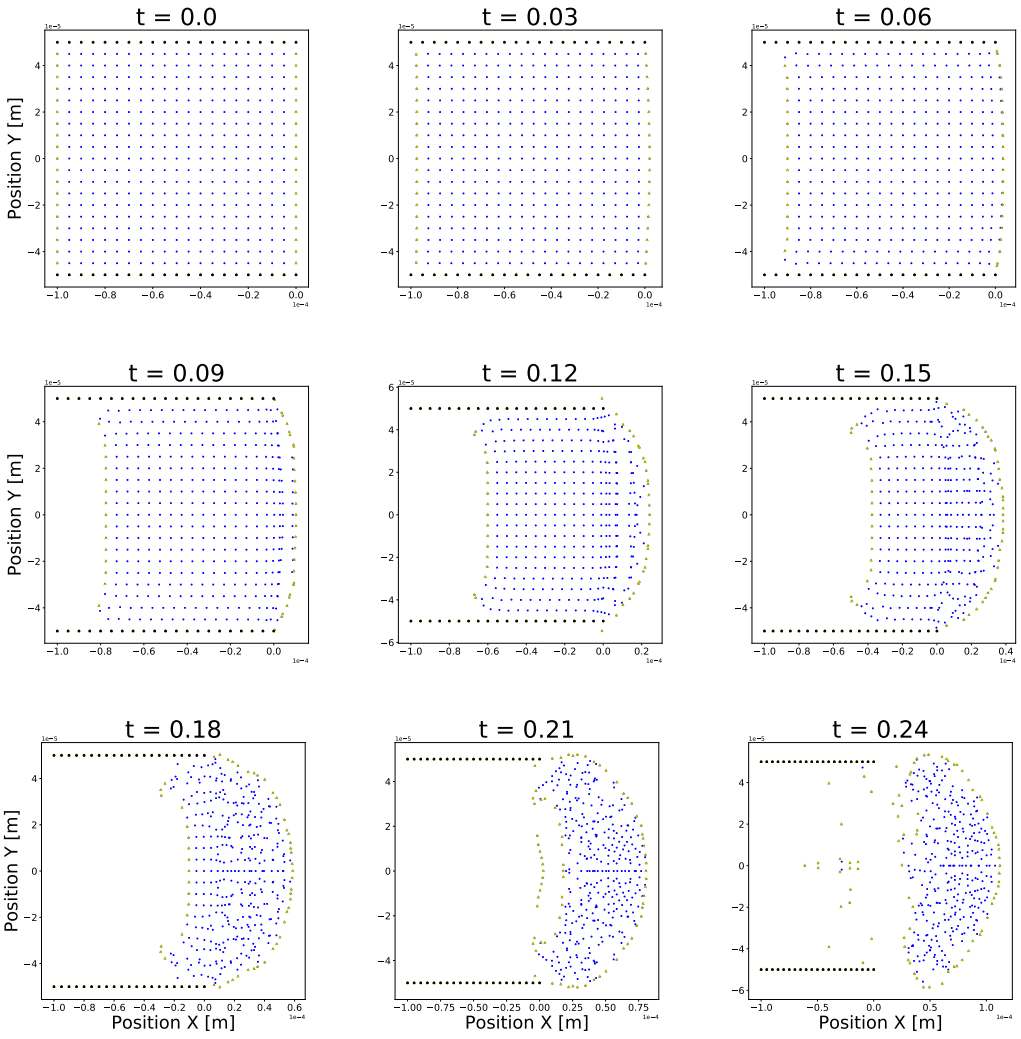

Figure 9. Simulation results for the heptane at extraction voltage of 8kV.

Based on the results, it is possible to observe the effect of surface tension over time. Additionally, as the fluid leaves the emitter, it is possible to observe some particles detaching. It is believed that this effect occurs because it is not possible to define an appropriate curvature radius using the method proposed by Sun *et al.* (2021) when the particle has zero or just one neighbor. In these cases, the surface tension was forced to zero, allowing the particle to leave the fluid without difficulty.

Furthermore, the problem was successfully resolved by employing various values of E_n. It was observed that the stability limit, $0.5\epsilon E_n^2 = \gamma\kappa$, held true. However, during certain conditions close to equilibrium, the algorithm encountered instabilities. An example is shown in Figure 10. The underlying causes of these instabilities remain unclear. One

aspect worth investigating is the influence of the ΔH parameter in the electrospray model. Additionally, other factors to consider include the impact of surface particles within the fluid and the presence of surface particles with just one or no neighboring particles where κ and $\hat{n}$ cannot be defined.

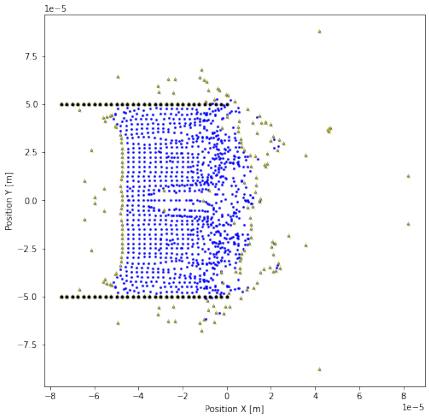

Figure 10. Example of unstable solution using 31×41 particles and a ratio between the surface and electrical force of 1.10.

4. CONCLUSION

In this paper, a Python-based Smoothed Particle Hydrodynamics (SPH) method was presented for simulating planar electrospray propulsion systems. Although maintaining a constant electric force over time enables the decoupling between the electrical problem and the fluid dynamics, this approximation tends to overestimate the force since the field intensity tends to vary with the fluid position. Nonetheless, the proposed approach is crucial for evaluating the developed tools as it encompasses all relevant elements of the electrospray problem.

The problem was solved using the open-source Scientific Computing Python Library. The choice of the solution method has an impact not only on the quality of the solution but also on the execution time. The results obtained for the Poiseuille and square droplet problems indicate that the RK45 method achieves a favorable balance between these two factors.

Regarding the particle search scheme, the hash table provides a simple yet efficient algorithm to identify the neighbours. The results demonstrate that the performance remains robust irrespective of the chosen grid cell size.

For the surface tension model, the approach adopted in Sun *et al.* (2021) was employed. This method performs well for the square droplet problem. However some instabilities were observed during the electrospray simulations, requiring further investigation.

Finally, as a future direction, the model will be modified to accommodate axisymmetric geometries and time-varying electric fields.

5. ACKNOWLEDGEMENTS

This study was financed in part by the Coordenação de Aperfeiçoamento de Pessoal de Nível Superior - Brasil (CAPES) - Finance Code 001 and the Fundação de Amparo à Pesquisa de Minas Gerais (FAPEMIG). The fourth author also acknowledges CNPq under the grant $406589/2022-4$.

6. REFERENCES

Adami, S., Hu, X. and Adams, N.A., 2010. "A new surface-tension formulation for multi-phase sph using a reproducing divergence approximation". *Journal of Computational Physics*, Vol. 229, No. 13, pp. 5011–5021.

Asher, J., Huang, Z., Cui, C. and Wang, J., 2022. "Multi-scale modeling of ionic electrospray emission". *Journal of Applied Physics*, Vol. 131, No. 1, p. 014902.

Band, S., Gissler, C. and Teschner, M., 2020. "Compressed neighbour lists for sph". *Computer Graphics Forum*, Vol. 39, No. 1, pp. 531–542. doi:https://doi.org/10.1111/cgf.13890.

Brackbill, J.U., Kothe, D.B. and Zemach, C., 1992. "A continuum method for modeling surface tension". *Journal of computational physics*, Vol. 100, No. 2, pp. 335–354.

Breinlinger, T., Polfer, P., Hashibon, A. and Kraft, T., 2013. "Surface tension and wetting effects with smoothed particle hydrodynamics". *Journal of Computational Physics*, Vol. 243, pp. 14–27.

Chong, C., Maolin, C. and Haohao, Z., 2020. "Characterization of an ionic liquid electrospray thruster with a porous

ceramic emitter". *Plasma Science and Technology*, Vol. 22, No. 9, p. 094009.

Gamero-Castaño, M., 2008. "The structure of electrospray beams in vacuum". *Journal of Fluid Mechanics*, Vol. 604, pp. 339–368.

Hu, L., Fuzhen, C., Ping, W., Fengshan, W. and Hongfu, Q., 2021. "Simulating electrohydrodynamics with smoothed particle hydrodynamics based on a charge-conservative approach". *Engineering Analysis with Boundary Elements*, Vol. 124, pp. 41–51.

Huh, H. and Wirz, R.E., 2019. "Numerical simulation of electrospray thruster extraction". In *Proceedings of the 36th International Electric Propulsion Conference, Vienna, Austria*. pp. 15–20.

Kim, D.Y. and Micci, M.M., 2013. "Molecular dynamics simulations of a liquid gallium electrospray thruster". *Journal of Propulsion and Power*, Vol. 29, No. 4, pp. 899–905.

Kundu, P.K., Cohen, I.M. and Dowling, D.R., 2015. *Fluid mechanics*. Academic press.

Legge Jr, R.S., 2008. "18.086 final project: Finite element modelling of ionic liquid flow through porous electrospray emitters".

Lev, D., Myers, R.M., Lemmer, K.M., Kolbeck, J., Koizumi, H. and Polzin, K., 2019. "The technological and commercial expansion of electric propulsion". *Acta Astronautica*, Vol. 159, pp. 213–227.

Lin, Y., Liu, G. and Wang, G., 2019. "A particle-based free surface detection method and its application to the surface tension effects simulation in smoothed particle hydrodynamics (sph)". *Journal of Computational Physics*, Vol. 383, pp. 196–206.

Liu, G.R., 2009. *Meshfree methods: moving beyond the finite element method*. CRC press.

Liu, G.R. and Liu, M.B., 2003. *Smoothed particle hydrodynamics: a meshfree particle method*. World scientific.

Liu, M. and Liu, G., 2010. "Smoothed particle hydrodynamics (sph): an overview and recent developments". *Archives of computational methods in engineering*, Vol. 17, pp. 25–76.

Logg, A., Mardal, K.A. and Wells, G., 2012. *Automated Solution of Differential Equations by the Finite Element Method*. Springer Berlin, Heidelberg.

Lozano, P.C., Martínez-Sánchez, M. and Hruby, V., 2010. "Electrospray propulsion". *Encyclopedia of Aerospace Engineering*.

Machado, K.D., 2007. *Teoria do eletromagnetismo: volume 1*. UEPG.

Mazouffre, S., 2016. "Electric propulsion for satellites and spacecraft: established technologies and novel approaches". *Plasma Sources Science and Technology*, Vol. 25, No. 3, p. 033002.

Monaghan, J.J., 1994. "Simulating free surface flows with sph". *Journal of computational physics*, Vol. 110, No. 2, pp. 399–406.

Morris, J.P., Fox, P.J. and Zhu, Y., 1997. "Modeling low reynolds number incompressible flows using sph". *Journal of computational physics*, Vol. 136, No. 1, pp. 214–226.

O'Reilly, D., Herdrich, G. and Kavanagh, D.F., 2021. "Electric propulsion methods for small satellites: A review". *Aerospace*, Vol. 8, No. 1, p. 22.

Reitz, J.R., 2009. *Foundations of electromagnetic theory*. Pearson Education India.

Scipy, 2023. "Fundamental algorithms for scientific computing in python". `https://scipy.org/`.

Sun, W., Zhang, L. and Liew, K., 2021. "Fast detection of free surface and surface tension modelling via single-phase sph". *Applied Mathematical Modelling*, Vol. 100, pp. 33–54.

Thuppul, A., Wright, P.L., Collins, A.L., Ziemer, J.K. and Wirz, R.E., 2020. "Lifetime considerations for electrospray thrusters". *Aerospace*, Vol. 7, No. 8, p. 108.

Uchizono, N., Collins, A., Marrese-Reading, C., Arestie, S., Ziemer, J. and Wirz, R., 2021. "The role of secondary species emission in vacuum facility effects for electrospray thrusters". *Journal of Applied Physics*, Vol. 130, No. 14, p. 143301.

White, F.M., 1966. *Fluid mechanics*.

Wirz, R.E., 2019. "Electrospray thruster performance and lifetime investigation for the lisa mission". In *AIAA Propulsion and Energy 2019 Forum*. p. 3816.

Xue, S., Duan, L. and Kang, Q., 2021. "Study on the emitter infiltration of needle-capillary ionic liquid electrospray thruster". *AIP Advances*, Vol. 11, No. 3, p. 035234.

7. RESPONSIBILITY NOTICE

The authors are solely responsible for the printed material included in this paper.